The Cryosphere Discuss., 9, 3055–3074, 2015
www.the-cryosphere-discuss.net/9/3055/2015/
doi:10.5194/tcd-9-3055-2015

The Cryosphere Discussions
Open Access

Photopolarimetric retrievals of snow properties

M. Ottaviani[1], B. van Diedenhoven[1,2], and B. Cairns[1]

[1]NASA Goddard Institute for Space Studies, 2880 Broadway, New York, NY, USA
[2]Center for Climate System Research, Columbia University, New York, NY, USA

Received: 28 March 2015 – Accepted: 6 May 2015 – Published: 29 May 2015

Correspondence to: M. Ottaviani (matteo.ottaviani@nasa.gov)

Published by Copernicus Publications on behalf of the European Geosciences Union.

Abstract

Polarimetric observations of snow surfaces, obtained in the 410–2264 nm range with the Research Scanning Polarimeter onboard the NASA ER-2 high-altitude aircraft, are analyzed and presented. These novel measurements are of interest to the remote sensing community because the overwhelming brightness of snow plagues aerosol and cloud retrievals based on air- and space-borne total reflection measurements. The spectral signatures of the polarized reflectance of snow are therefore worthwhile investigating in order to provide guidance for the adaptation of algorithms currently employed for the retrieval of aerosol properties over soil and vegetated surfaces. At the same time, the increased information content of polarimetric measurements allows for a meaningful characterization of the snow medium. In our case, the grains are modeled as hexagonal prisms of variable aspect ratios and microscale roughness, yielding retrievals of the grains' scattering asymmetry parameter, shape and size. The results agree with our previous findings based on a more limited dataset, with the majority of retrievals leading to moderately rough crystals of extreme aspect ratios, for each scene corresponding to a single value of the asymmetry parameter.

1 Introduction

The development of accurate techniques for the retrieval of climatologically relevant parameters in snow-covered regions is of obvious importance for the success of climate models predictions (Comiso, 2006; Zwally and Giovinetto, 2011; Zatko et al., 2013). For instance, the retrieval of grain size and surface temperature leads to information that can be used to map the snow melting state, valuable to understand the mass balance of the ice sheets (Stamnes et al., 2007; Lyapustin et al., 2009). Passive optical sensors are employed in this regard to evince the optical and microphysical properties of snow grains from measurements of snow reflectance, and advanced algorithms have been applied to data collected by the MODerate resolution Imaging Spectroradiometer

TCD
9, 3055–3074, 2015

(MODIS) and sensors with similar capabilities (Hori et al., 2007; Aoki et al., 2007; Jin et al., 2008; Stamnes et al., 2011). However, the limited information content of such measurements translates into uniqueness problems during the retrieval process, with the result that operational snow products are still limited to snow covered area and albedo (with the exception of the recent addition to MODIS of the dust radiative forcing product as described in Painter et al., 2012). Polarimetric remote sensing (Diner et al., 2007; Cairns et al., 2009; Dubovik et al., 2011; Hasekamp et al., 2011; Chowdhary et al., 2012; Ottaviani et al., 2012a; Knobelspiesse et al., 2012) adds to the information contained in MODIS-type observations because it can provide information on the ice grain shape (van Diedenhoven et al., 2012; Ottaviani et al., 2012b) and an accurate characterization of the optical and microphysical properties of aerosols present in the scene including possible impurities embedded in the snowpack. The benefits of passive polarimetric observations originate from both their extreme sensitivity to particle microphysics and the specifics of surface polarized reflectance. For conventional land types (soil, vegetation), the latter can be effectively parameterized as a scaled Fresnel reflection function with negligible spectral dependence. As a consequence, the separation of the signal into its surface and atmospheric contributions (i.e., the atmospheric correction procedure) is achieved with improved accuracy.

The NASA GISS Research Scanning Polarimeter (RSP, Cairns et al., 1999), born as an aerosol research instrument, collects a target's total and polarized reflectance with high accuracy in 9 bands between 410 and 2264 nm and at 152 viewing angles per scene. A recent deployment led to the first published study of the polarimetric signatures of snow reflectance from airborne observations (Ottaviani et al. (2012b), hereafter referred to as O12). In that case, the measurements were acquired over a topologically complex terrain in the Yosemite National Park region and processed with an automated, iterative atmospheric correction scheme purposely created to analyze the spectral dependence of the polarized reflectance. A preliminary retrieval of crystal microphysical and optical properties was also tested. The purpose of this new work is to apply the same atmospheric correction procedure and to extend the surface properties

TCD
9, 3055–3074, 2015

retrieval scheme to a more recent dataset of improved quality, in terms of the flatness of the surveyed terrain.

In the next section we describe the data collection, and in Sect. 3 the processing scheme. In Sect. 4 we discuss the results obtained from the analysis. The conclusions are found in Sect. 5.

2 Data

The data analyzed here were collected onboard the high-altitude ER-2 aircraft during the POlarimeter Definition EXperiment (PODEX) mission, a NASA effort to ultimately test and compare the performance of different polarimeters, as part of the Decadal Survey activities and in preparation of the Studies of Emissions and Atmospheric Composition, Clouds and Climate Coupling by Regional Surveys (SEAC4RS) campaign. Compared to more traditional aircraft such as the King Air B200 used in O12, the ER-2 offers the advantages of a perspective more similar to that of a satellite. For example, interference caused by cirrus clouds is readily assessed using the RSP 1880 nm channel, which is usually very dark because of the strong absorption by tropospheric water vapor that masks the surface, and is therefore very sensitive to high-altitude clouds. There is in fact interest in exploiting this wavelength as a cirrus screener in a broader context, since cold places tend to have dry atmospheres and the reflectance of snow at 1880 nm is much less than at, say, 1380 nm (the effective strength of absorption by ice at 1880 nm is twice that exhibited at 1380 nm). Also, RSP operations on the ER-2 benefit from the stable attitude intrinsic to stratospheric flights, which enhances data quality since the RSP scans along the flight track (approximately 50° on either side of nadir) to assemble the multiangle view of a target's reflectance from subsequent scans.

About a dozen snow-covered targets were selected for the 6.8 h flight over Colorado and the Sierra Nevada range in California on 15 March 2012. Well-formed snowpacks with little to no interference from vegetation and flatness of terrain were the main priorities. Three scenes were chosen for this analysis. The Grand Mesa plateau

TCD
9, 3055–3074, 2015

(39°08′ N, 108°12′ W, ∼ 3000 m a.s.l.) in Western Colorado exhibits remarkable flatness and a consistent snowpack with a depth of greater than one meter from nearly simultaneous in-situ surveys (Mesa Lakes SNOTEL site managed by the Natural Resources and Conservation Service of the US Department of Agriculture, and M. Skiles, personal communication, 2013). Lake Granby (40°10′ N, 105°53′ W, ∼ 2500 m a.s.l.), the third largest body of water in Colorado and second largest reservoir, was frozen at the time of the overpass and covered with a thin layer of aged, likely metamorphosed snow (the SNOTEL site at Stillwater Creek reports a snow depth of ∼ 0.5 m). The scene denoted by Derby Peak (39°59′ N, 107°10′ W, ∼ 3500 m a.s.l.) is another high-altitude rather flat region (in fact belonging to the Flat Tops Wilderness Area). The closest SNOTEL site at Trapper Lake, 2950 m a.s.l., reports a snow depth of 0.7 m.

3 Methodology

The details of the method employed for the atmospheric correction procedure are explained in detail in O12. In short, the Jacobians generated from the linearization of the Doubling-Adding radiative transfer code in use at GISS (De Haan et al., 1987) are used to separate the surface and atmospheric signals within an iterative scheme based on a general inversion and optimization procedure (Rodgers, 2000). This iterative scheme decouples the surface and the atmospheric contributions of the total signal measured at instrument altitude, while expressing the surface total reflectance as the weighted sum of three kernels as in the RossThick – LiSparse form (Wanner et al., 1995; Lucht et al., 2000):

$$R(\Theta) = f_{\mathrm{iso}} + f_{\mathrm{vol}} K_{\mathrm{vol}}(\Theta) + f_{\mathrm{geo}} K_{\mathrm{geo}}(\Theta) \quad (1)$$

where Θ is the scattering angle. The three terms on the right-hand side describe different scattering mechanisms: a Lambertian component for isotropic reflection, a volumetric term K_{vol} for scattering from small structures and a geometric term K_{geo} for

TCD
9, 3055–3074, 2015

a macroscopic shadowing from large objects. Although this model was created for reflection from surfaces other than snow, its mathematical form adapts without problems to snowpacks, with the isotropic kernel systematically assuming the largest weight because of the dominance of multiple scattering in the reflection of light from snow.

As far as the polarized reflectance is concerned, we instead employ a scaled Fresnel kernel elsewhere used for vegetated surfaces (Nadal and Bréon, 1999):

$$R_{\mathrm{p}} = \frac{F_{\mathrm{p}}(\theta_{\mathrm{i}})}{4[\cos(\theta_s) + \cos(\theta_v)]} \tag{2}$$

with the fractional polarized reflectance $F_{\mathrm{p}}(\theta_{\mathrm{i}})$ given by (Born and Wolf, 1999):

$$F_{\mathrm{p}}(\theta_{\mathrm{i}}) = \frac{1}{2}\left[\left(\frac{n_1\cos\theta_{\mathrm{i}} - n_2\cos\theta_t}{n_1\cos\theta_{\mathrm{i}} + n_2\cos\theta_t}\right)^2 - \left(\frac{n_2\cos\theta_{\mathrm{i}} - n_1\cos\theta_t}{n_2\cos\theta_{\mathrm{i}} + n_1\cos\theta_t}\right)^2\right] \tag{3}$$

where n_1 and n_2 are the indices of refraction of pure air and ice, and the angle of refraction θ_t is connected to the angle of incidence θ_{i} by Snell's law.

Shifting the attention to the retrieval of crystal habit, the polarized reflectance at 864 nm is used because of the very weak ice absorption at this wavelength and the relatively weak Rayleigh scattering contribution. In these retrievals, the fit is sought to the RSP measurements by using a database of ice crystal properties to implement the radiative transfer within the snow layer. Limited by the lack of constraints on the correct optical properties, very few studies have departed from the common practice of assuming spherical shapes for the snow grains, an approximation which can negatively impact the quality of the albedo products (Tedesco and Kokhanovsky, 2007; Aoki et al., 2000). In our case, the description of the snowpack is refined by treating it as a compact, optically semi-infinite medium composed of ice crystals modeled as hexagonal prisms with variable aspect ratios and microscale facet roughness. It should be noted that for the remote sensing of aerosols over snow, a model capable of accurately reproducing the contribution of the surface to the total signal should be considered successful

TCD
9, 3055–3074, 2015

regardless of its capability to mimic the true shape of the crystals. There is recognition that hexagonal plates and columns can be effectively used as radiative proxies for more complex crystal habits (Fu, 2007; Baran, 2009; van Diedenhoven et al., 2012; Ottaviani et al., 2012a). As demonstrated by van Diedenhoven et al. (2012), matching measured polarized reflectances with simulated values by adjusting the aspect ratios and roughness parameters of simple hexagonal particles yields an estimate of the asymmetry parameter of the more complex ice crystals within the top of the snowpack. Our database, initially created to be of use for the retrieval of ice clouds properties, contains 765 different combinations of aspect ratios and roughness parameters and was computationally assembled by running Monte Carlo simulations based on geometric optics (Macke et al., 1996). The use of conventional geometric optics and the simple parameterization of rough crystals were evaluated by van Diedenhoven et al. (2012).

The retrieval of grain size is instead based on the total reflectance at selected Short-Wave InfraRed (SWIR) bands where ice absorption is high. The total reflectance of an optically semi-infinite snow layer at 2264 and 1594 nm is effectively determined by the asymmetry parameter and the single scattering albedo at the respective wavelength. The single scattering albedo at a given wavelength in turn is mainly determined by the effective diameter of the ice crystals. The grain diameter is not unequivocally defined in the literature, which is understandable since the definition of snow grain itself is often ambiguous. There is a consensus for expressing grain effective diameter as proportional to the ratio of crystal volume to projected area, but the value of the multiplier can vary according to the specific choice of the author (Kokhanovsky et al., 2011; Kokhanovsky and Zege, 2004; Aoki et al., 2000). In line with several recent publications (see for example Zege et al., 2011; Jin et al., 2008), we define it as 3/2 times the ratio of their volume over the crystal surface area as outlined in the Appendix, which includes the details of the relationship to geometric size. Here, we estimate the effective diameter of snow for a given scene by matching the measured reflectance with a simulated value assuming an ice crystal model with an asymmetry parameter consistent with the asymmetry parameter retrieved for that scene using the method described above. To

TCD
9, 3055–3074, 2015

this end, various modified gamma size distributions were applied to yield varying effective diameters and the doubling-adding radiative transfer code was used to simulate the corresponding 1594 and 2264 nm reflectances (van Diedenhoven et al., 2014). For conditions equivalent to those found in snowpacks, Bi et al. (2014) showed that the errors in retrieved effective radius attributable to the use of the conventional geometric optics approach are below 5 %. In the analysis, it should be remembered that the 1594 and 2264 nm channels experience different penetration depths, with the former weighted more towards the top layer while the latter probes deeper into the medium: as a consequence, the retrieved sizes contain information on the vertical structure of the snowpack (Wang et al., 2009; Li et al., 2001; Warren, 1982).

As far as the atmospheric component is concerned, the high elevation of these alpine scenes allowed us to assume negligible contributions from aerosols, so that in the radiative transfer code a standard Rayleigh atmosphere was used with a surface pressure extrapolated at the indicated altitude. Cirrus-free conditions were guaranteed from the screening procedure described earlier. The SWIR channels were corrected for the minimal interference caused by absorption from a standard amount of trace gases.

There certainly is debate on the applicability of the radiative transfer theory to a densely packed medium as snow. In any case, the formalism is recognized to model the total reflectance with sufficient accuracy for reasons likely associated with the large number of scattering events taking place within the snowpack. Based on this assumption, the method is expected to perform even better for the polarization component because the polarimetric signatures of a medium are known to originate from its top layer (van Diedenhoven et al., 2013): deeper into the medium (i.e., past the first units of optical depth) multiple scattering randomizes polarization.

4 Results and discussion

The core of our findings is condensed in Fig. 1. The analysis for each scene (different columns in the figure) was performed over a single RSP pixel, corresponding to a spa-

TCD
9, 3055–3074, 2015

tial resolution of about 225 m, since averaging over a few adjacent aggregated scans did not show appreciable scan-to-scan variability, revealing more or less uniform snow conditions within the instrument instantaneous field of view. The upper panels show the results of the iterative correction scheme applied to the relevant RSP channels. With the exception of O12, the visible and SWIR behavior of the polarized reflectance of snow has not been previously published. Real-time imagery from the high-resolution camera onboard the ER-2, overlaid to Google Earth, is included for context.

The total reflectance exhibits the familiar high spectral albedo in the visible, although with some expected scene-to-scene variability. Lake Granby in particular shows lower total reflectance than the other two scenes; in situ simultaneous surveys from the personnel at the US Forest Service in Arapaho National Forest reported a snow depth on the order of 5–8 cm. These values are close to the limit of thickness required to visually mask the underlying surface, leaving the possibility that the lake ice underneath the snow cover is darkening the reflectance. Nevertheless, it should be remembered that a layer of a few millimeters is sufficient to fulfill the semi-infinite approximation at the long wavelengths used for the retrieval of grain size. Conversely, the SWIR channels at 1594 and 2264 nm are very dark as expected by the strong absorption of ice at these wavelengths. The polarized reflectance as a function of the scattering angle is very similar among the three scenes. Note that in the case of Derby Peak the flight track was oriented at about 45° with respect to the principal plane (i.e. the plane defined by the solar azimuth and the normal to the surface), leading to a smaller range of scattering angles collected by the RSP. It has already been observed in O12 as the land model used for the polarized reflectance converges to zero toward backscatter (scattering angle > 160°), and in this region agreement with the data is not to be expected. It is useful to quantify the spectral spread of the channels by examining the differences from the reference 2264 nm channel. The signal in this band is in fact a proxy for the surface contribution, since the Rayleigh (and fine-mode aerosol) contribution becomes more and more negligible as the observation windows shifts to the SWIR. If the spectral differences are small, that same signal can then be subtracted from the shorter RSP

TCD
9, 3055–3074, 2015

wavelengths when aerosols retrievals are attempted. The residuals with respect to the 2264 nm polarized reflectance are found to be within 0.005, which as in O12 is larger than conventional land surfaces but still very small. The polarized reflectance is small too in absolute value.

Shifting the attention to the search of a snow model, the plots at the bottom contour the Root Mean Square Error (RMSE) of the data fit to each combination of aspect ratio and roughness parameter in the database. Multiple combinations led to a satisfactory fit to each of the three polarized reflectance observations, so we considered as optimal all habits with an RMSE falling below a small threshold value (4.5×10^{-7}). These minima, marked with red circles, therefore correspond to those crystal habits that when used to model the snowpack at the bottom of the simulated atmosphere yield the best fits to the data. The analysis shows that the polarized reflectances are consistent with particles that have components that are like thin plates or like thin columns, a fact already observed in O12. Interestingly, the butterfly-like topology of the RMSE was recognized to closely resemble that obtained for the asymmetry parameter g plotted vs. the same coordinates (Fig. 2). In each scene, the optimal crystal habits are associated with very similar values of the asymmetry parameter (0.84 for Lake Granby, 0.876 for Derby Peak and 0.90 for Grand Mesa). This result is understood by considering that the asymmetry parameter is the main descriptor for the scattering properties. As demonstrated by van Diedenhoven et al. (2012) using a large variety of complex ice crystal shapes, all the combinations of aspect ratio and roughness parameter fitting a polarized reflectance measurement are ultimately characterized by similar values of g. Consequently, they will also yield similar particles size retrievals.

All retrieved parameters are conveniently reported for comparison in Table 1, together with the results of the size retrievals. Using the simple approach outlined in the previous section, we obtained effective diameters equal to 152, 182 and 144 µm for the Grand Mesa, Lake Granby and Derby Peak scene, respectively, when using the RSP band at 2264 nm. Using instead the 1594 nm channel, diameters typically 30 µm smaller are obtained for each scene, which can be explained by the different

TCD
9, 3055–3074, 2015

penetration depths of the two channels, indicating crystal size increasing with depth as expected (Hori et al., 2007; Li et al., 2001; Aoki et al., 2000; Warren, 1982). These values, at the lower end of common retrieval ranges, are normally associated with fresh snow conditions as found in studies based on other remote sensors in alpine regions (Negi and Kokhanovsky, 2011; Painter et al., 2009; Dozier and Painter, 2004; Nolin and Dozier, 2000) and polar plateaus (Lyapustin et al., 2009; Hori et al., 2007). However, a direct comparison is challenged by differences in the definition of grain size, assumptions on grain sphericity and different penetration depths achieved by the use of selected instrument channels. The larger grain sizes obtained for the Lake Granby scene were attributed to the shallow aged snow over the lake, since metamorphized snow is recognized to be composed of larger grains (Aoki et al., 2000; Warren, 1982).

5 Conclusions

We have presented the extension of a novel analysis described by Ottaviani et al. (2012b) to a dataset acquired with the high-accuracy RSP airborne instrument overflying high-altitude snow fields. The data were processed within an automated retrieval scheme capable of isolating the surface contribution. The spectral dependence of the polarized reflectance is larger than for soil or vegetated surfaces, but nonetheless small. This fact has important implications for the construction of advanced algorithms which aim at the retrieval of the microphysical properties of aerosols layers located over ice and snow fields.

Furthermore, we applied a retrieval procedure which is demonstrated to yield snow microphysical parameters of primary climatological interest. We retrieve snowpacks behaving as a collection of grains of extreme geometries (thin plates and/or long columns) and moderate to high microscale roughness. These results reinforce those of our previous study based on a limited dataset acquired over very rugged terrain. For each scene, the best fits are obtained for a set of crystal habits characterized by very simi-

TCD
9, 3055–3074, 2015

lar values of the asymmetry parameter. Size retrievals were also tested, leading grain effective diameters in the 140–180 µm range.

Appendix: Size descriptors for hexagonal prisms

The results of Macke's Geometric Optics code were tabulated with the choice of the radius of the sphere with equal surface area, r_{sph}, as a size descriptor. This parameter is linked to the geometric size of hexagonal prisms and to the grain effective diameter by the following relations:

$$A_{hex} = 4\,\pi\,r_{sph}^2 \qquad \text{(Surface area of sphere and hexagonal prism)} \qquad \text{(A1)}$$

$$A_p = A_{hex}/4 = \pi\,r_{sph}^2 \qquad \text{(Projected surface area of hexagonal prism)} \qquad \text{(A2)}$$

$$r_{hex} = \sqrt{\frac{4\,A_p}{3\,\sqrt{3}+12\,\alpha}} \qquad \text{(Radius or side length of hexagonal prism)} \qquad \text{(A3)}$$

$$V = 3\,\sqrt{3}\,\alpha\,r_{hex}^3 \qquad \text{(Volume of hexagonal prism)} \qquad \text{(A4)}$$

$$d_{eff} = \frac{3}{2}\frac{V}{A_p} = \frac{6\sqrt{3}\alpha}{\sqrt{3}+4\alpha}r_{hex} \qquad \text{(Effective diameter)} \qquad \text{(A5)}$$

where α is the aspect ratio, defined as the ratio of the cross section width of the prism to its length. The last expression is valid for a single particle of any solid shape. In case of a polydisperse collection of particles, the effective diameter is obtained through integration over a size distribution:

$$D_{eff} = \frac{3}{2}\frac{\int_0^\infty V(D)\,N(D)\,\mathrm{d}D}{\int_0^\infty A_p(D)\,N(D)\,\mathrm{d}D} \qquad \text{(A6)}$$

with N denoting the number density of crystals with maximum dimension D, which can be defined as $2\,r_{hex}$ for plates and $2\,\alpha\,r_{hex}$ for columns.

TCD
9, 3055–3074, 2015

Acknowledgements. This work was possible through the dedication of the ER-2 pilots Tom Ryan, Dean Neeley and Stu Broce. Their exceptional skills and proactive attitude towards the goals of the mission were critical to success. The assistance of personnel on the ground was invaluable, especially that of Hans Moosmüller from the Desert Research Institute, Davide Sartoni from Mistras-Ropeworks, Rick Brinkam from Water Services at the City of Grand Junction, Sam Williams and Aldin Strautins from NOAA, McKenzie Skiles from NASA JPL, Holly King from the Trappers Lake Lodge, and Dan Matthews and John Saye from the US Forest Service in Arapaho National Forest. We also thank Rose Dominguez and Dennis Gearhart from NASA GSFC for providing access to the ER-2 DCS camera imagery. The RSP data used for this analysis are publicly available on the GISS server (http://data.giss.nasa.gov/pub/rsp/). The graphs were produced with IDL© supplemented by David Fanning's Coyote Graphics free library of routines. Partial support from the Radiation Sciences Program managed by Hal Maring is gratefully acknowledged.

References

Aoki, T., Aoki, T., Fukabori, M., Hachikubo, A., Tachibana, Y., and Nishio, F.: Effects of snow physical parameters on spectral albedo and bidirectional reflectance of snow surface, J. Geophys. Res., 105, 10219–10236, 2000. 3060, 3061, 3065

Aoki, T., Hori, M., Motoyoshi, H., Tanikawa, T., Hachikubo, A., Sugiura, K., Yasunari, T. J., Storvold, R., Eide, H. A., Stamnes, K., Li, W., Nieke, J., Nakajima, Y., and Takahashi, F.: ADEOS-II/GLI snow/ice products – Part II: Validation results using GLI and MODIS data, Remote Sens. Environ., 111, 274–290, 2007. 3057

Baran, A.: A review of the light scattering properties of cirrus, J. Quant. Spectrosc. Ra., 110, 1239–1260, 2009. 3061

Bi, L., Yang, P., Liu, C., Yi, B., Baum, B. A., van Diedenhoven, B., and Iwabuchi, H.: Assessment of the accuracy of the conventional ray-tracing technique: Implications in remote sensing and radiative transfer involving ice clouds, J. Quant. Spectrosc. Ra., 158–174, 2014. 3062

Born, M. and Wolf, E.: Principles of Optics, 7th (expanded) Edn., Cambridge University Press, 1999. 3060

Cairns, B., Russell, E., and Travis, L.: Research scanning polarimeter: calibration and ground-based measurements, in: Society of Photo-Optical Instrumentation Engineers (SPIE) Con-

TCD
9, 3055–3074, 2015

ference Series, Vol. 3754, edited by: Goldstein, D. H. and Chenault, D. B., Denver, CO, USA, 18 July 1999, 186–196, 1999. 3057
Cairns, B., Waquet, F., Knobelspiesse, K., Chowdhary, J., and Deuzé, J.: Polarimetric remote sensing of aerosols over land surfaces, Chap. 10, Springer-Praxis Books in Environmental Sciences, Chichester, UK, 295–325, 2009. 3057
Chowdhary, J., Cairns, B., Waquet, F., Knobelspiesse, K., Ottaviani, M., Redemann, J., Travis, L., and Mishchenko, M.: Sensitivity of multiangle, multispectral polarimetric remote sensing over open oceans to water-leaving radiance: analyses of RSP data acquired during the MILAGRO campaign, Remote Sens. Environ., 118, 284–308, doi:10.1016/j.rse.2011.11.003, 2012. 3057
Comiso, J. C.: Arctic warming signals from satellite observations, Weather, 61, 70–76, 2006. 3056
De Haan, J., Bosma, P., and Hovenier, J.: The adding method for multiple scattering calculations of polarized light, Astron. Astrophys., 183, 371–391, 1987. 3059
Diner, D. J., Davis, A., Hancock, B., Gutt, G., Chipman, R. A., and Cairns, B.: Dual-photoelastic-modulator-based polarimetric imaging concept for aerosol remote sensing, Appl. Optics, 46, 8428–8445, 2007. 3057
Dozier, J. and Painter, T.: Multispectral and hyperspectral remote sensing of alpine snow properties, Annu. Rev. Earth Pl. Sc., 32, 465–494, 2004. 3065
Dubovik, O., Herman, M., Holdak, A., Lapyonok, T., Tanré, D., Deuzé, J. L., Ducos, F., Sinyuk, A., and Lopatin, A.: Statistically optimized inversion algorithm for enhanced retrieval of aerosol properties from spectral multi-angle polarimetric satellite observations, Atmos. Meas. Tech., 4, 975–1018, doi:10.5194/amt-4-975-2011, 2011. 3057
Fu, Q.: A new parameterization of an asymmetry factor of cirrus clouds for climate models, J. Atmos. Sci., 64, 4140–4150, 2007. 3061
Hasekamp, O. P., Litvinov, P., and Butz, A.: Aerosol properties over the ocean from parasol multiangle photopolarimetric measurements, J. Geophys. Res., 116, D14204, doi:10.1029/2010JD015469, 2011. 3057
Hori, M., Aoki, T., Stamnes, K., and Li, W.: ADEOS-II/GLI snow/ice products – Part III: Retrieved results, Remote Sens. Environ., 111, 291–336, 2007. 3057, 3065
Jin, Z., Charlock, T., Yang, P., Xie, Y., and Miller, W.: Snow optical properties for different particle shapes with application to snow grain size retrieval and MODIS/CERES radiance comparison over Antarctica, Remote Sens. Environ., 112, 3563–3581, 2008. 3057, 3061

TCD
9, 3055–3074, 2015

Knobelspiesse, K., Cairns, B., Mishchenko, M., Chowdhary, J., Tsigaridis, K., van Diedenhoven, B., Martin, W., Ottaviani, M., and Alexandrov, M.: Analysis of fine-mode aerosol retrieval capabilities by different passive remote sensing instrument designs, Opt. Express, 20, 21457–21484, 2012. 3057

Kokhanovsky, A. and Zege, E.: Scattering optics of snow, Appl. Optics, 43, 1589–1602, 2004. 3061

Kokhanovsky, A., Rozanov, V., Aoki, T., Odermatt, D., Brockmann, C., Krüger, O., Bouvet, M., Drusch, M., and Hori, M.: Sizing snow grains using backscattered solar light, Int. J. Remote Sens., 32, 6975–7008, 2011. 3061

Li, W., Stamnes, K., Chen, B., and Xiong, X.: Snow grain size retrieved from near-infrared radiances at multiple wavelengths, Geophys. Res. Lett., 28, 1699–1702, 2001. 3062, 3065

Lucht, W., Schaaf, C., and Strahler, A.: An algorithm for the retrieval of albedo from space using semiempirical BRDF models, IEEE T. Geosci. Remote, 38, 977–998, 2000. 3059

Lyapustin, A., Tedesco, M., Wang, Y., Aoki, T., Hori, M., and Kokhanovsky, A.: Retrieval of snow grain size over Greenland from MODIS, Remote Sens. Environ., 113, 1976–1987, 2009. 3056, 3065

Macke, A., Mueller, J., and Raschke, E.: Single scattering properties of atmospheric ice crystals, J. Atmos. Sci., 53, 2813–2825, 1996. 3061

Nadal, F. and Bréon, F.-M.: Parameterization of surface polarized reflectance derived from POLDER spaceborne measurements, IEEE T. Geosci. Remote, 37, 1709–1718, 1999. 3060

Negi, H. S. and Kokhanovsky, A.: Retrieval of snow grain size and albedo of western Himalayan snow cover using satellite data, The Cryosphere, 5, 831–847, doi:10.5194/tc-5-831-2011, 2011. 3065

Nolin, A. and Dozier, J.: A hyperspectral method for remotely sensing the grain size of snow, Remote Sens. Environ., 74, 207–216, 2000. 3065

Ottaviani, M., Cairns, B., Chowdhary, J., Diedenhoven, B. V., Knobelspiesse, K., Hostetler, C., Ferrare, R., Burton, S., Hair, J., Obland, M. D., and Rogers, R.: Polarimetric retrievals of surface and cirrus clouds properties in the region affected by the Deepwater Horizon oil spill, Remote Sens. Environ., 121, 389–403, doi:10.1016/j.rse.2012.02.016, 2012a. 3057, 3061

Ottaviani, M., Cairns, B., Ferrare, R., and Rogers, R.: Iterative atmospheric correction scheme and the polarization color of alpine snow, J. Quant. Spectrosc. Ra., 113, 789–804, doi:10.1016/j.jqsrt.2012.03.014, 2012b. 3057, 3065

TCD
9, 3055–3074, 2015

Painter, T., Rittger, K., McKenzie, C., Slaughter, P., Davis, R., and Dozier, J.: Retrieval of subpixel snow covered area, grain size, and albedo from MODIS, Remote Sens. Environ., 113, 868–879, 2009. 3065

Painter, T. H., Bryant, A. C., and Skiles, S. M.: Radiative forcing by light absorbing impurities in snow from MODIS surface reflectance data, Geophys. Res. Lett., 39, L17502, doi:10.1029/2012GL052457, 2012. 3057

Rodgers, C.: Inverse methods for atmospheric sounding theory and practice, Vol. 2, in: Series on Atmospheric, Oceanic and Planetary Physics, World Scientific Publishing Company, Singapore, 2000. 3059

Stamnes, K., Li, W., Eide, H., Aoki, T., Hori, M., and Storvold, R.: ADEOS-II/GLI snow/ice products – Part I: Scientific basis, Remote Sens. Environ., 111, 258–273, 2007. 3056

Stamnes, K., Hamre, B., Stamnes, J., Ryzhikov, G., Biryulina, M., Mahoney, R., Hauss, B., and Sei, A.: Modeling of radiation transport in coupled atmosphere-snow-ice-ocean systems, J. Quant. Spectrosc. Ra., 112, 714–726, doi:10.1016/j.jqsrt.2010.06.006, 2011. 3057

Tedesco, M. and Kokhanovsky, A.: The semi-analytical snow retrieval algorithm and its application to MODIS data, Remote Sens. Environ., 111, 228–241, 2007. 3060

van Diedenhoven, B., Cairns, B., Geogdzhayev, I. V., Fridlind, A. M., Ackerman, A. S., Yang, P., and Baum, B. A.: Remote sensing of ice crystal asymmetry parameter using multi-directional polarization measurements – Part 1: Methodology and evaluation with simulated measurements, Atmos. Meas. Tech., 5, 2361–2374, doi:10.5194/amt-5-2361-2012, 2012. 3057, 3061, 3064

van Diedenhoven, B., Cairns, B., Fridlind, A. M., Ackerman, A. S., and Garrett, T. J.: Remote sensing of ice crystal asymmetry parameter using multi-directional polarization measurements – Part 2: Application to the Research Scanning Polarimeter, Atmos. Chem. Phys., 13, 3185–3203, doi:10.5194/acp-13-3185-2013, 2013. 3062

van Diedenhoven, B., Fridlind, A. M., Cairns, B., and Ackerman, A. S.: Variation of ice crystal size, shape, and asymmetry parameter in tops of tropical deep convective clouds, J. Geophys. Res.-Atmos., 119, 11–809, 2014. 3062

Wang, X., Liou, K., Ou, S. S., Mace, G., and Deng, M.: Remote sensing of cirrus cloud vertical size profile using MODIS data, J. Geophys. Res.-Atmos., 114, D09205, doi:10.1029/2008JD011327, 2009. 3062

Wanner, W., Li, X., and Strahler, A.: On the derivation of kernels for kernel-driven models of bidirectional reflectance, J. Geophys. Res., 100, 21077–21089, 1995. 3059

TCD
9, 3055–3074, 2015

Warren, S.: Optical properties of snow, Rev. Geophys., 20, 67–89, 1982. 3062, 3065
Zatko, M. C., Grenfell, T. C., Alexander, B., Doherty, S. J., Thomas, J. L., and Yang, X.: The influence of snow grain size and impurities on the vertical profiles of actinic flux and associated NO_x emissions on the Antarctic and Greenland ice sheets, Atmos. Chem. Phys., 13, 3547–3567, doi:10.5194/acp-13-3547-2013, 2013. 3056
Zege, E., Katsev, I., Malinka, A., Prikhach, A., Heygster, G., and Wiebe, H.: Algorithm for retrieval of the effective snow grain size and pollution amount from satellite measurements, Remote Sens. Environ., 115, 2674–2685, 2011. 3061
Zwally, H. J. and Giovinetto, M. B.: Overview and assessment of Antarctic ice-sheet mass balance estimates: 1992–2009, Surv. Geophys., 32, 351–376, 2011. 3056

TCD
9, 3055–3074, 2015

Table 1. List of ice crystals' parameters retrieved for the three analyzed scenes. The value in parentheses indicates the RSP band used in the retrieval. The effective diameter can be obtained using either the 2264 or the 1594 nm channel (see text), and a crystal habit characterized by the asymmetry parameter retrieved for the corresponding scene.

Retrieved Parameter	Grand Mesa	Lake Granby	Derby Peak
Asymmetry parameter (864 nm)	0.90	0.84	0.876
Aspect ratio (864 nm)	< 0.08	< 0.05	< 0.2, >10
Roughness parameter (864 nm)	0.3–0.5	0.6–0.7	0.2–0.6
Effective diameter (2264 nm)	152 µm	182 µm	144 µm
Effective diameter (1594 nm)	122 µm	152 µm	114 µm

TCD
9, 3055–3074, 2015

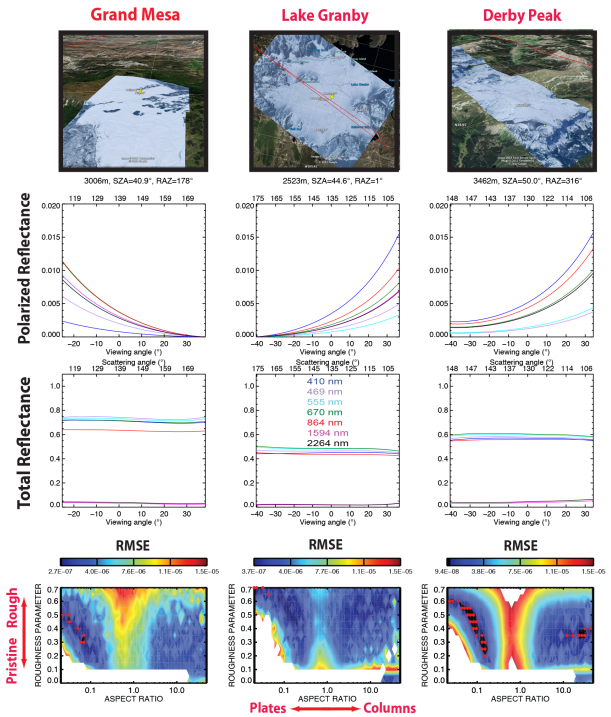

Figure 1. Atmospherically corrected polarized (*second row*) and total (*third row*) reflectance for three snow fields (*columns*) overflown in Colorado, USA. The first row shows real-time imagery from the high-resolution camera onboard the ER-2. The last row pertains to the search of the optimal ice grain model for each scene: the contour plots map the RMSE of the fit to the polarized reflectance at 864 nm when simulating the snowpack with each crystal habit (i.e., each combination of aspect ratio and roughness parameter) in the database. The red circles locate the values of the RMSE falling under a predetermined threshold, and are taken to represent the retrieved (optimal) habits.

TCD
9, 3055–3074, 2015

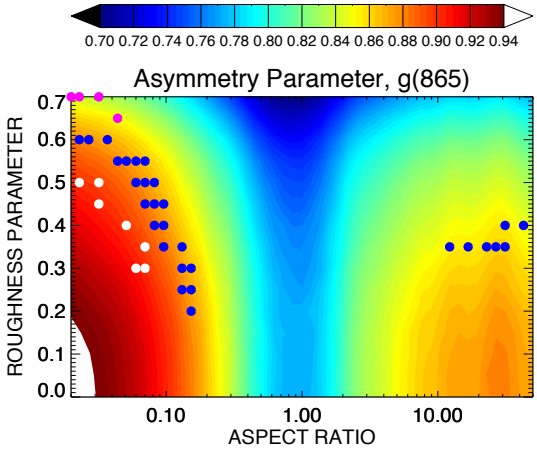

Figure 2. The "butterfly" pattern of the contour plot for the asymmetry parameter g as a function of aspect ratio and roughness parameter resembles that obtained for the RMSE plots in Fig. 1. The red circles in Fig. 1 (here in white for Grand Mesa, magenta for Lake Granby and blue for Derby Peak) that identify the retrieved optimal crystal habits are found for each scene clustered around a single value of g.

TCD
9, 3055–3074, 2015